

NLP-enabled trajectory map-matching in urban road networks using transformer sequence-to-sequence model

Sevin Mohammadi¹, and Andrew W. Smyth^{*2}

Abstract—Large-scale geolocation telematics data acquired from connected vehicles has the potential to significantly enhance mobility infrastructures and operational systems within smart cities. To effectively utilize this data, it is essential to accurately match the geolocation data to the road segments. However, this matching is often not trivial due to the low sampling rate and errors exacerbated by multipath effects in urban environments. Traditionally, statistical modeling techniques such as Hidden-Markov models incorporating domain knowledge into the matching process have been extensively used for map-matching tasks. However, rule-based map-matching tasks are noise-sensitive and inefficient in processing large-scale trajectory data. Deep learning techniques directly learn the relationship between observed data and road networks from the data, often without the need for hand-crafted rules or domain knowledge. This renders them an efficient approach for map-matching large-scale datasets and more robust to the noise. This paper introduces a sequence-to-sequence deep-learning model, specifically the transformer-based encoder-decoder model, to perform as a surrogate for map-matching algorithms. The encoder-decoder architecture initially encodes the series of noisy GPS points into a representation that automatically captures autoregressive behavior and spatial correlations between GPS points. Subsequently, the decoder associates data points with the road network features and thus transforms these representations into a sequence of road segments. The model is trained and evaluated using GPS traces collected in Manhattan, New York. Achieving an accuracy of 76%, transformer-based encoder-decoder models extensively employed in natural language processing presented a promising performance for translating noisy GPS data to the navigated routes in urban road networks.

Index Terms—map-matching, telematics data, GPS, GNSS, the transformer, sequence-to-sequence modeling, encoder-decoder, deep Learning.

I. INTRODUCTION

The emergence of smart cities and Intelligent Transportation Systems (ITS) marks a significant advancement in urban mobility planning and management [1]. Leveraging advanced technologies, these systems propel the development of transportation infrastructures [2], enhance traffic safety [3]–[5], contribute to the growth of intelligent and sustainable cities [6]. Central to this paradigm are Connected Vehicles

(CVs), which enable Vehicle-to-Vehicle (V2V) and Vehicle-to-Infrastructure (V2I) communication, creating a network for intelligent urban navigation [7]. The ubiquity of communication technologies has facilitated the collection of large amounts of real-world data, ranging from vehicle speed and location to traffic conditions. Leveraging the knowledge acquired from connected vehicles opens opportunities to gain new insights into driving behavior that enhances traffic predictions [8] and traffic safety [5]. Among the pool of data gathered by connected vehicles, the trajectory data derived from geolocation information holds numerous applications encompassing monitoring transportation systems and urban infrastructure, safety management [5], [9], [10], public transit efficiency improvement [11], [12], ride-hailing services [13], travel time prediction for operational systems [14], [15], and optimizing emergency response systems [16], [17]. By tracking the movement of vehicles, trajectory data facilitates route optimization and the identification of congestion zones and enhances the efficiency of urban road networks. Markovi et al. review trajectory data applications in different domains such as modeling human behavior, designing public transit, traffic performance measurement and prediction, environment, and safety [18].

Nevertheless, accurately deducing vehicle trajectories from noisy geolocation data obtained through Global Navigation Satellite Systems (GNSS) has become a key concern. In dense urban environments such as New York City, the abundance of tall buildings and narrow streets introduces complexities that challenge GNSS data collection. Obstacles like signal loss, reflections, and multipath interference introduce a significant source of error in GPS data, compromising the reliable and accurate representation of vehicular trajectory [19]. Figure 1 illustrates a multipath signal and compares the resultant erroneous path against the actual route on the map. Moreover, the quality of recovered routes is compromised by low sampling rates, measurement errors, and atmospheric conditions. Therefore, one of the major challenges in GPS trajectory data utilization pertains to handling noisy and imprecise GPS records.

Map-matching is a crucial process in transportation and geospatial data analysis that assigns measured GPS locations to specific road segments or locations on a map. Map-matching algorithms mostly rely on a combination of sensor data, including GPS coordinates, speed, and heading, and map data, such as road network topology and lane configurations. These algorithms employ a wide range of techniques spanning from statistical techniques to data-driven approaches,

¹Sevin Mohammadi is Graduate Research Assistant in the Department of Civil Engineering and Engineering Mechanics, Columbia University, New York, NY 10027, USA (sm4894@columbia.edu)

²Andrew W. Smyth (corresponding author) is the Robert A. W. and Christine S. Carleton Professor of Civil Engineering and Engineering Mechanics and the Director of the Center for the Smart Streetscapes (CS3), Columbia University, New York, NY 10027, USA (aws16@columbia.edu)

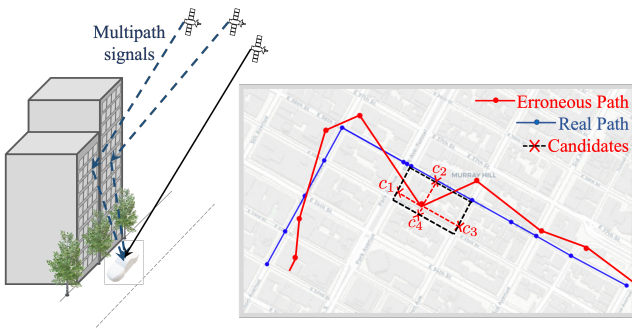


Fig. 1. Left: Illustration of signal reflections caused by tall buildings in an urban environment, leading to multipath errors. Right: Comparison between the erroneous path in red and the actual path in blue within Manhattan. Map-matching accurately estimates the true path. The illustration provides an example of all candidate segments, denoted as C_1, C_2, C_3, C_4 , for one of the erroneous raw GPS points collected off the road segment.

encompassing geometric algorithms, probabilistic models, and various advanced models [20], [21]. These techniques are employed to estimate the accurate positions and, consequently, to identify the most probable path or route taken by a vehicle or individual.

Refining noisy GPS points to align them with consecutive road segments through advanced map-matching algorithms primarily involves a series of sophisticated and often challenging rules and techniques. An essential preliminary step, shared by many algorithms, involves the selection of candidate road segments for each observed GPS point (Figure 1 shows an example), then one seeks the most likely path among the set of all possible routes. Typically, road segments that fall within a confidence region often represented as an ellipse or a circle centered around the GPS point, are chosen as candidate roads. The dimension of the confidence region is determined based on the positioning error statistics, which is either a fixed distance threshold or an adaptive region [22]. How the path is estimated from the candidate segments varies depending on the particular map-matching algorithm being used. Different algorithms employ their unique strategies for choosing the most likely path based on the set of candidate segments.

However, with the increasing number of vehicles equipped with GPS devices that collect massive data, there is a growing need for a more efficient and scalable map-matching solution. Traditional map-matching tasks often involve a series of complex rules and data processing, making them inefficient, especially when confronted with large datasets or intricate algorithms. Deep learning surrogate models offer a promising solution to this challenge. In the context of map matching, a deep learning surrogate model refers to a neural network model crafted to replicate complex and often computationally demanding map-matching algorithms. Its purpose is to serve as a substitute for the original matching procedure, primarily aiming to accelerate and streamline the task while enhancing accuracy. By harnessing the wealth of historical trajectory data, data-driven algorithms are capable of discerning underlying mobility patterns and noise structures reflected by the data. Therefore, deep learning models autonomously discover the mapping function between input data (e.g., GPS coordinates)

and output data (e.g., matched road segments) in an end-to-end manner. This task simplification reduces the necessity for extensive feature engineering, facilitating the alignment of GPS points with the road segments. Therefore, it yields a reliable tool for identifying trajectories within the road network.

This paper introduces a deep-learning model, in particular the transformer-based encoder-decoder model, to serve as a surrogate for advanced, rule-based map-matching algorithms. In particular, the transformer model that utilizes a self-attention mechanism in an encoder-decoder architecture [23] is trained to map the input sequence of GPS points onto a sequence of road segments. In the encoder-decoder architecture, the encoder initially encodes the noisy GPS points into a representation that captures the autoregressive behavior and spatial correlation between GPS points. Subsequently, the decoder captures the relationship between these GPS points and the road network features and thus transforms this representation into a sequence of road segments. The proposed deep-learning sequence-to-sequence model is a powerful technique capable of learning the most complex spatial-temporal characteristics of the data and the noise pattern across the road network from a large amount of trajectory data.

II. RELATED WORKS

In this section, a brief review of existing map-matching algorithms is presented. More comprehensive reviews of these algorithms are provided by [20], [21], [24], [25]. Early map-matching algorithms were primarily search-based, focusing on the identification of the nearest road segment to a raw GPS point based solely on the geometry of the road segments [26], [27]. This approach, known as geometric map-matching, disregarded the connectivity of the roads. However, with further advancements, topological matching algorithms were introduced, which took into account the contiguity of geometric shapes [28], [29]. Building upon these developments, researchers then proposed probabilistic algorithms that relied on GPS error statistics to establish a confidence region [30], [31]. This error region enabled the selection of multiple candidate segments, each to be evaluated using different criteria.

These pioneering studies formed the basis for the subsequently advanced map-matching algorithms that utilize sophisticated techniques, such as Hidden Markov Models (HMM) [32]–[35], and weight-graph technique [28], [36]–[38], Kalman Filter [39], [40], Fuzzy logic models [41], [42]. Weight-based algorithms and HMMs are among the widely used algorithms. Weight-based map-matching algorithms typically assign scores to candidate road segment pairs, considering factors like spatial proximity, vehicle heading relative to segment direction, link connectivity, and turn restrictions at junctions [38]. These algorithms then select consecutive segments forming a least-cost path using methods like Dijkstra’s shortest-path algorithm [43]. In HMM-based map-matching, where hidden states correspond to the road segments, the goal is to determine the most likely sequence of hidden states given a sequence of observations (here GPS points), typically accomplished through the use of the Viterbi

algorithm [44]. HMMs model the sequence of states as a discrete-time Markov chain, where transitions to the next state depend solely on the current state. This reflects the Markov property that simplifies the modeling of dependencies between states. HMMs maximize the joint probability of the observed sequence and the hidden sequence by combining the emission probabilities and transition probabilities. The emission probability quantifies the likelihood of observing noisy GPS points given the vehicle’s presence in a candidate segment. The transition probability represents the conditional likelihood of transitioning from one hidden state to another, equivalent to transitioning from one road segment to the next segment. It captures the dynamics of how the hidden states evolve over time in the Markov chain. Some map-matching algorithms employ a combination of weight-based models and HMMs that transforms the HMM problem into a Dijkstra least-cost path problem. They construct a virtual graph with candidate points as nodes and interconnecting paths as edges, assigning costs based on computed joint probabilities [22], [35].

However, a significant drawback of map-matching algorithms is their limited ability to effectively leverage historical data, rendering them vulnerable to noisy input. Deep learning-based map-matching models, in contrast, leverage large trajectory data during training which enables them to capture intricate patterns including noise and mobility within extensive trajectories, and thus makes them robust to noise. By learning complex representations from the data, these models effectively harness historical information, leading to significant improvements in map-matching performance while offering the advantage of efficient processing of large data. This combination of robustness, and efficient processing makes deep learning models valuable for map-matching task. The prevalent deep learning architecture for map-matching vehicle trajectories includes the sequence-to-sequence (seq2seq) models, which often incorporate an encoder-decoder structure including recurrent neural networks (RNNs) [45]–[47] and graph neural networks [48]. RNN-based seq2seq models are priorly used for vehicle trajectory prediction [49], space-free vehicle trajectory recovery [50], and human mobility prediction [51]. Later, Feng et al. utilized an RNN-based seq2seq model in particular LSTM-based encoder-decoder named DeepMM for map-matching. They enhanced their model’s performance by applying data augmentation techniques that simulated the generation process of real-like raw trajectories. This approach allowed them to generate a substantial number of virtual trajectories from ground truth trajectories, thereby enriching their training dataset [45]. Although simulated trajectories enriches the training data, it overlooks the role of the underlying driving pattern and route choice behavior of the drivers. Ren et al. implemented a multi-task seq2seq learning architecture in particular GRU-based encoder-decoder named MTrajRec to predict the road segment and the moving ratios for each GPS point simultaneously [46]. Moreover, Jian et al. harnessed a seq2seq GRU-based RNN model to refine the map-matching results for low-quality trajectory data by integrating data distribution learning from high-frequency trajectories and incorporating an explicit mobility pattern recognition module

into their deep learning algorithm [47]. This approach sets their work apart from other deep learning map-matching algorithms, which rely on the deep model’s capacity to extract embedded mobility patterns from extensive trajectory data. In the context of seq2seq encoder-decoder models used for map-matching, RNNs have historically played a central role. However, there are inherent drawbacks associated with training RNN models. One well-known challenge is the vanishing or exploding gradient problem, which can hinder training effectiveness. Additionally, RNN-based encoder-decoder models incur high computational costs, particularly when processing lengthy sequences, making the processing of long sequences a limitation.

In this paper, we solve the map-matching task by constructing a seq2seq model based on the transformer architecture [23]. In this model, the RNN component is replaced with multiple self-attention modules in both the encoder and decoder, allowing the model to significantly outpace RNN-based encoder-decoder models in terms of accuracy and speed, particularly when processing a large set of lengthy GPS trajectories in urban network.

III. MAP-MATCHING

A. Map-matching preliminaries

This section outlines the definitions of the key components of the map-matching task and describes the format of the raw and matched data for the purpose of this paper.

Map-matching is a technique designed to determine the sequence of connected road segments on a digital road network map that best approximates the actual route taken by a vehicle, even in the presence of errors and noise in the observed GPS data. This task is challenging, especially in an urban environment, due to the significant positioning errors and the complex, dense road map. In our study, the map-matching algorithm takes a sequence of observed coordinates in raw GPS data as input and produces a segment-based trajectory as the output. However, the low sampling rate in data collection leads to a sparse input representation. Consequently, no direct one-to-one correspondence exists between observed GPS points and inferred road segments.

Raw GPS Trajectory is a collection of timestamped, noisy data points recorded by a GPS device at a frequency determined by the device setting. The sampling rate may vary depending on the purpose of the data collection and the capacity of the data storage infrastructure, resulting in either low or high sampling trajectory data. The collected data points typically include information about the vehicle’s position, such as latitude, longitude, altitude, and vehicle speed, as well as additional information, such as the number of satellites with which the GPS device communicates during location sampling. For the map-matching task in this study, the raw GPS trajectory is defined as a sequence order of latitude and longitude pairs, denoted by $T = \{(x_1, y_1), (x_2, y_2), \dots, (x_n, y_n)\}$. Here, (x_i, y_i) represents the coordinates of the location points, and n is the number of collected points along the route.

Segment-based Trajectory is a chronological sequence of connected road segments that accurately represents the

vehicle’s path. In map-matching, a “road segment” is a portion of a digital road map corresponding to a particular stretch of road in the actual road network. When a GPS device records a vehicle’s position, the recorded latitude and longitude points are not perfectly aligned with the road segments on the digital map due to errors and noise.

Digital Map. A digital map or digital road network is a form of map data that is typically represented by a directed graph. The set of nodes represents the intersections or endpoints of the road segments, while the set of directed edges connects these nodes. In this graph representation, each directed edge corresponds to a road segment, with its direction indicating the allowed direction of traffic along the segment. By using this graph representation, map-matching algorithms accurately identify the segment-based trajectory from raw GPS trajectory.

IV. METHODOLOGY

A. Problem Statement

This paper aims to develop a surrogate model for the map-matching tasks. The goal is to create a deep learning model that estimates the actual route taken by a vehicle in the form of a sequence of road segments when provided with a sequence of sparse, raw GPS coordinates. A seq2seq model is a well-suited approach to achieve this objective. This study employs a transformer-based encoder-decoder model to predict the most likely route based on a sequence of spatially unique grid cells onto which the noisy raw coordinates are projected.

B. Seq2seq Model

A Seq2seq model with neural network [52] is an architecture commonly used in natural language processing (NLP) for various tasks such as machine translation, text summarizing, conversation generation, and in other fields that involve sequential data such as image captioning, music generation, and drug discovery [53]. The basic idea behind seq2seq models is to take a sequence of input tokens and generate a sequence of output tokens corresponding to the input sequence. The most common architecture for seq2seq models is the encoder-decoder. The encoder extracts the important features of the input sequence and produces continuous representations of the input that summarize all relevant information. Then, the decoder recursively generates the output sequence one element at a time based on the decoded context and the previously generated element. The key advantage of seq2seq models is their ability to handle variable-length input and output sequences, which makes them well-suited for tasks where the length of the input and output sequences can vary. Additionally, the neural network-based seq2seq models are capable of learning complex patterns and interdependencies within sequential data, yielding enhanced performance compared to conventional neural network models. RNN and the transformers are the most common model architectures used in the encoder-decoder models. However, the vanishing or exploding gradient problem is a well-known challenge in training RNN encoder-decoder models. This issue arises when the gradients used for backpropagation become extremely small or large, causing the model to fail to converge effectively.

In addition to the vanishing or exploding gradient problem, RNN encoder-decoder models are computationally expensive, especially for long sequences. Attention mechanisms mitigate gradient problems in RNN encoder-decoder models, enhancing performance, especially with long sequences, by focusing on specific input parts during output generation. Nevertheless, RNN encoder-decoder models with attention mechanisms remain computationally demanding due to the added computational overhead required for calculating attention weights for each input token. The transformers are a newer model architecture introduced by [23] that addresses the limitations of RNN encoder-decoder models. Transformers diverge from RNNs in their architecture, opting instead for stacks of self-attention mechanisms to capture the interconnections within input sequences and their relevance to output sequences. The decoder component leverages parallelized matrix multiplications, simultaneously processing all input sequence elements, as opposed to the sequential nature of RNNs. This parallel processing is a pivotal factor contributing to transformers’ enhanced speed and efficiency compared to traditional RNN-based models, which tend to have a more sequential processing approach, often leading to extended training times and slower inference speeds. Additionally, the transformers have been shown to achieve the state-of-the-art performance on a variety of tasks [23].

C. Objective Function

Let $g = (g_1, g_2, \dots, g_n)$ be the transformed version of $T = \{(x_1, y_1), (x_2, y_2), \dots, (x_n, y_n)\}$, representing the variable-length input sequence, here in this study, a sequence of grid cells, each of which encompasses each GPS point, and $r = (r_1, r_2, \dots, r_m)$ be the variable-length output sequence, i.e., sequence of road segments, m is the length of the output sequence. The seq2seq model maps g to r by learning a conditional probability distribution over the set of possible output sequences, given the input sequence.

$$p(r|g) = \prod_{t=1}^m p(r_t|r_1, \dots, r_{t-1}, g)$$

The model learns a probability distribution from input-output pairs in training, adjusting parameters to maximize output sequence likelihood given input; the seq2seq model aims to maximize this log-likelihood.

$$\begin{aligned} \arg \max_{\theta} P(r|g) &= \arg \max \log P(r|g) \\ &= \arg \max \sum_{t=1}^m \log P(r_t|g_n, r_{<t}). \end{aligned}$$

The objective can be optimized using backpropagation of cross-entropy loss through time, which computes the gradients of the objective with respect to the model parameters and updates the parameters using gradient descent. Once the model is trained, it can be used to generate segment-based trajectories for new input sequences.

In particular, the transformer [23] is employed in the seq2seq model to build the surrogate model for mapping g to r .

D. The Transformer

The neural network architecture with the transformer, depicted in Figure 2, comprises two primary components: the encoder and the decoder. Detailed explanations of each component are provided in the subsequent sections.

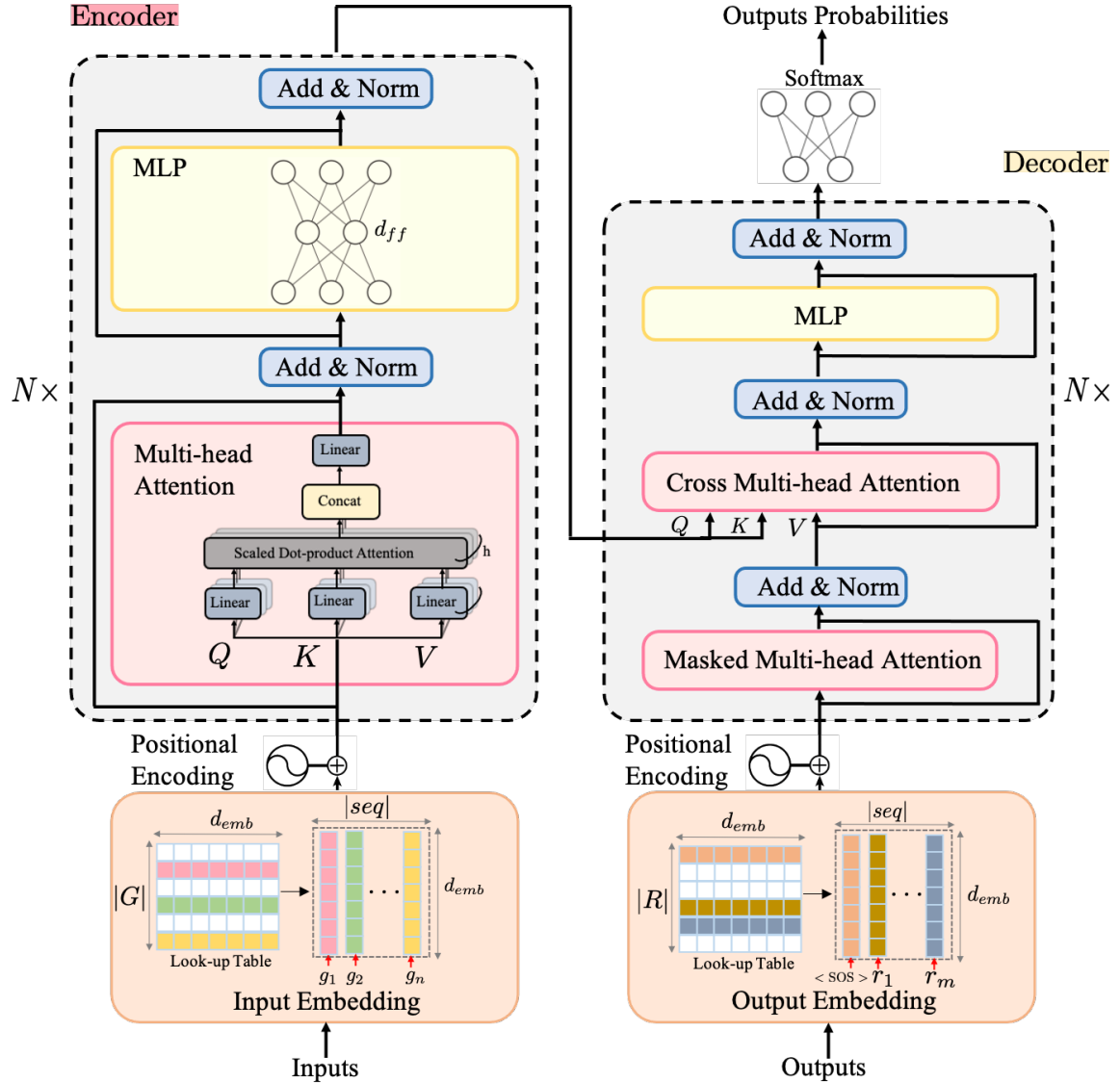


Fig. 2. Transformer Model. The encoder on the left and the decoder on the right both contain an embedding layer followed by positional encoding and N transformer blocks. $|G|$ and $|R|$ are the size of unique grids and unique road segments in the region (counterpart of vocabulary size in NLP). d_{emb} , d_{mlp} , N , and h are the model hyperparameters.

1) *Encoder*: The encoder in the transformer is composed of an embedding layer, a positional encoding layer, and a stack of N identical layers, each layer composed of a multi-head self-attention mechanism, and a position-wise fully connected feed-forward neural network each of which is followed by a normalization residual connection layer (*Add & Norm*), each of which is explained in details as follows.

Embedding. The input to the proposed surrogate map-matching model is a sequence of grid cells encompassing the original GPS points. These grid cells are obtained by partitioning the entire road network into uniform square sections, and the sequence of these grid cells aligns with the sequence of the GPS points (details explained in the preprocessing section). Every grid cell is assigned a unique numerical index, which is then translated to a fixed-size one-hot vector. Consequently, the one-hot vector is typically long but sparse. The size of the

one-hot vectors, represented by $|G|$, aligns with the number of distinct cells in the region, including two additional labels to mark the sequence's beginning and the end. The equivalent of $|G|$ in NLP is the source vocabulary size. The embedding layer consists of a trainable embedding matrix operating similarly to a lookup table that correlates an embedding vector with each distinct grid cell. These embedding vectors are learned during the training process of the neural network.

Positional Encoding. Within this layer, the positional encoding matrix is generated for the input embedding matrix, and subsequently, it is incorporated into the embedded matrix by matrix addition. Given that, unlike recurrent neural networks (RNNs), the transformer architecture lacks the innate ability to capture the order of the elements in the sequence, an additional mechanism is required to infuse positional context into the model. Positional encoding informs the transformer

about token positions in a sequence, aiding in distinguishing elements by their sequence order, which is essential for tasks where element arrangement matters. The positional encoding utilizes a set of fixed sinusoidal functions with different frequencies to represent the position of individual tokens within the sequence. These sinusoidal functions are combined with the token embeddings to generate the final input representation encompassing semantic and positional context. We use the same formula for calculating the positional encoding proposed in [23], which is as follows:

$$PE_{(pos,i)} = \sin\left(\frac{pos}{10000^{\frac{2i}{d_{emb}}}}\right),$$

$$PE_{(pos,2i+1)} = \cos\left(\frac{pos}{10000^{\frac{2i}{d_{emb}}}}\right),$$

where $pos \in \{1, \dots, n\}$ is the position of the token in the sequence of length n , $i \in \{1, \dots, d_{emb}\}$ is the dimension of the positional encoding, d_{emb} is the model's embedding dimension also referred as model dimension.

Multi-head Attention. Multi-head attention allows the model to focus on different parts of the input sequence simultaneously and learn different aspects of the data in parallel. A multi-head attention layer takes three identical copies of the output of the positional encoding layer or the previous self-attention layer as the query matrix denoted as (Q), the key matrix denoted as (K), and the value matrix denoted as (V). The query matrix represents the elements from the previous layer that are being used to generate attention scores for each element in the current layer. Each row of the query matrix is a query vector corresponding to each sequence element. Similarly, the key matrix represents elements from the previous layer. It consists of key vectors, each corresponding to an element in the sequence, and is used to determine how well other elements match or relate to the corresponding query vectors. Key vectors are crucial in computing attention scores, which indicate the importance of other elements for each query. Similarly, the value matrix represents elements from the previous layer and consists of value vectors that hold the information passed to the next layer. The attention scores calculated using query and key vectors determine how much weight each value vector receives when producing the output. Multi-head attention is a combination of n self-attentions. The most common self-attention involves calculating attention scores between the query and key matrices by taking the dot product of Q and K^T and then scaling the result by the square root of the dimension of the key vectors, d_k . Therefore, the core operation of self-attention is scaled dot-product attention. The attention scores are passed through the Softmax function to obtain attention weights. The attention weights are then used to compute a weighted sum of the value matrix (V). This aggregation process captures the relevant information from different elements in the input sequence based on their importance.

Multi-head attention applies linear transformations to map input into h lower-dimensional matrices such that $hd_k = d_{emb}$. The weight matrices of these transformations are learned during training. Therefore, in the multi-head attention mechanism, the scaled dot-product attention process is repeated h times, in parallel, each time using different linearly transformed versions of Q , K , and V . The outputs from these parallel at-

tention heads are concatenated and linearly transformed again to produce the final multi-head attention output. The following equations represent the operations in the mathematical format:

$$\text{Attention}(Q, K, V) = \text{Softmax}\left(\frac{QK^T}{\sqrt{d_k}}\right)V,$$

$$\text{Multi-head Attention} = \text{Concat}(\text{head}_1, \dots, \text{head}_h)W^o,$$

$$\text{head}_i = \text{Attention}(QW_i^Q, KW_i^K, VW_i^V),$$

where W_i^Q , W_i^K , W_i^V , and W^o are learnable weight matrices.

Normalization Residual Connection. Normalization Residual Connection layer (Add & Norm) is the transformer component that helps stabilize and improve the convergence of the training process. It is an element-wise addition of each sub-layer input and its output, followed by layer normalization [54], and it is used after every sub-layer in the transformer blocks within both the encoder and decoder. Layer normalization normalizes the values along each dimension of the input tensor. This helps to stabilize the training process and improve the flow of gradients during backpropagation.

Feed Forward Neural Network Layer. The transformer's feedforward neural network or multilayer perceptron consists of two main linear transformations with a Rectified Linear Unit (ReLU) activation function. The input to the feedforward network is the output from the previous layer. This input is passed through a linear transformation called the point-wise feedforward layer. It uses a weight matrix and a bias term to perform a linear mapping of each position separately and identically to a new intermediate representation, d_{ff} . After the first linear transformation, the ReLU activation function is applied to introduce non-linearity to the transformation. The result of the activation function is then passed through another linear transformation, similar to the first step. This transformation maps the intermediate representation to the final output with the model embedding dimension.

2) *Decoder:* The decoder in the transformer operates in an autoregressive manner, implying that it generates tokens sequentially, with each step's outcome contingent upon previously generated tokens. This process entails an iterative approach, where the generated token from each step is fed back into the decoder for subsequent steps. Similar to the encoder, the decoder contains an embedding layer, a positional encoding layer, and a stack of N identical layers, each encompasses a masked multi-head layer, a cross multi-head attention layer, and a feed-forward neural network layer. These components are subsequently followed by a normalization residual connection layer, concluding with a final linear layer connected to a Softmax function. In the decoder's self-attention, elements are masked to block access to subsequent elements, allowing the encoder to utilize input and prior output tokens but not tokens from the output sequence that follow the current position. The cross multi-head attention layer allows the model to look at and consider information from every position in the input sequence simultaneously and in turn captures the information in the input sequence that is pertinent or necessary for generating the current token in the output sequence. Indeed, the cross-multi-head attention assists the decoder in establishing alignment between the produced output and the relevant input context. This alignment is achieved by utilizing the previous layer of the decoder for queries (Q)

allowing the model to consider its own context, while the keys (K) and values (V) are sourced from the output of the encoder's final layer providing access to the input sequence. Consequently, every key-value pair signifies a distinct position within the input sequence.

V. EXPERIMENT

A. Baseline

1) *HMM*: The goal of this paper is to introduce robust surrogate modeling for map-matching. In particular, in this paper, we are building a transformer-based map-matching model to operate as a surrogate model for our in-house cost-based HMM map-matching engine. This engine incorporates an innovative map-matching algorithm that merges speed data from On-Board Diagnostics (OBD-II) sensor modules within the vehicles with the GPS trajectory data. This fusion yields a notable enhancement in robustness and accuracy, and the algorithm overperformed a reliable off-the-shelf map-matching platform, resulting in an accuracy of 97.45% [55].

2) *RNN-based encoder-decoder with attention mechanism*: We also compare the transformer-based map-matching model with the RNN-based encoder-decoder model. The RNN-based encoder-decoder model and its variants have been adopted by [45], [46]. Feng et al. trained and evaluated DeepMM, the LSTM-based encoder-decoder with attention mechanism, with the trajectory data generated and recorded in part of Beijing containing 4,058 road segments, and the sampling interval of 60 seconds. They achieved the highest accuracy of 66% [45]. Similarly, Ren et al. trained and evaluated MTrajRec, the GRU-based encoder-decoder with attention mechanism and multi-task learning component, with the trajectory data recorded in Jinan, Shandong with 2,571 road segments in the area, and they achieved the highest recall accuracy of 74.98% for the data with a high sampling rate and 69.72% for the data with a low-sampling rate [46]. In another research work, Liu et al. trained a graph-based encoder-decoder model with 64k trajectories collected in the northeast of Beijing with 8.5K road segments and achieved an accuracy of 66.22% for trajectories with 30-second time intervals. They have also shown that their model outperformed MTrajRec [48].

The main components of the RNN-based encoder-decoder architecture are two layers: the embedding layer and the RNN layer. Therefore, the main difference between the RNN-based encoder-decoder with the transformer-based encoder-decoder is its recurrent layer versus the self-attention layer in the transformer. The architecture of the RNN-based encoder-decoder model is presented in Figure 3. In an RNN-based encoder-decoder, during the encoding, the RNN layer processes all the tokens on the input sequence iteratively and reutilizes the hidden state of an iteration as the input for generating the hidden state for the next element. The last hidden state of the RNN is passed as input to the first iteration of the decoder. Therefore, when processing a sequence of inputs, the RNN layer generates a sequence of hidden states, with each hidden state being a function of the current input and the previous hidden state. In particular, a bidirectional Gated Recurrent Unit (Bi-GRU) in the RNN layer of the encoder, and

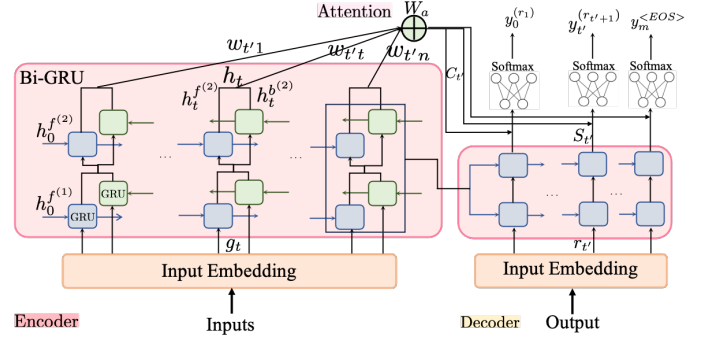


Fig. 3. Bi-GRU Encoder-Decoder

a regular GRU in the RNN layer of the decoder are utilized. The structure of the Gated Recurrent Unit (GRU) is presented in figure 4. GRU captures the sequential information in the

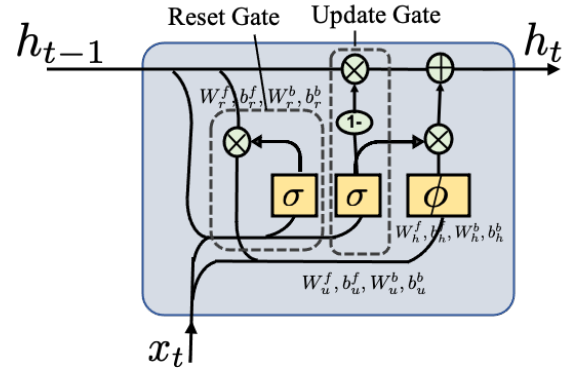


Fig. 4. Gated Recurrent Unit

data by maintaining an internal hidden state that evolves over time. It has a gating mechanism that controls the flow of information within the network, making it capable of learning and remembering longer sequences compared to traditional RNNs. The gating mechanism consists of an update gate and a reset gate, which control how much of the previous hidden state should be retained and how much new information should be incorporated in each time step.

A Bi-GRU is a variant of the GRU architecture that processes input sequences in both forward and backward directions. The input sequence is fed into two separate GRU layers, one processing the input sequence in the forward direction and the other processing the input sequence in the backward direction. The outputs of the two layers at each time step are concatenated and passed to the next layer or used as the final output. The architecture of the GRU cell is shown in figure 4.

The output of each direction of GRU, h_t , called hidden state at time step t , is a linear combination of the previous hidden state h_{t-1} and candidate activation \tilde{h}_t in which an update vector, u_t , controls the extent of the combination. The candidate activation \tilde{h}_t is a function of the input, x_t , and previous hidden state after going through the reset gates, and similarly, the update vector, u_t , is a function of the input and previous hidden state after going through the update gates. The equations that describe the GRU update process for forward

and backward GRU are as follows. The superscripts f and b denote the forward and backward recurrent components, respectively.

$$\begin{aligned} h_t^f &= (1 - u_t^f) * h_{t-1}^f + u_t^f * \tilde{h}_t^f, \\ \tilde{h}_t^f &= \phi(W_h^f[r_t^f * h_{t-1}^f, x_t] + b_h), \\ u_t^f &= \sigma(W_u^f[h_{t-1}^f, x_t] + b_u^f), \\ r_t^f &= \sigma(W_r^f[h_{t-1}^f, x_t] + b_r^f), \end{aligned}$$

$$\begin{aligned} h_t^b &= (1 - u_t^b) * h_{t+1}^b + u_t^b * \tilde{h}_t^b, \\ \tilde{h}_t^b &= \phi(W_h^b[r_t^b * h_{t+1}^b, x_t] + b_h^b), \\ r_t^b &= \sigma(W_r^b[h_{t+1}^b, x_t] + b_r^b), \\ u_t^b &= \sigma(W_u^b[h_{t+1}^b, x_t] + b_u^b), \end{aligned}$$

where r_t^f and r_t^b are reset vectors, u_t^f and u_t^b are update vectors, \tilde{h}_t^f and \tilde{h}_t^b are candidate activations, h_t^f and h_t^b are the hidden states. x_t is the current input, and t denotes the time step in the input sequence. σ and ϕ are the sigmoid and hyperbolic tangent activation functions, respectively. W_h , W_r , W_z , w_y are weight matrices associated with the input vectors and b_h , b_u , b_r are the biases which are the model's learnable parameters. The hidden states of the two forward and backward layers at each time step are concatenated to produce the final activation state, $h_t = [h_t^f, h_t^b]$.

In a regular encoder-decoder setup, a single hidden state is used to represent the entire input sequence and convey all the information from the encoder to the decoder. However, relying solely on this single vector can result in a loss of important information over time, as the information gets diluted by the time it reaches the final state of the encoder. To address this issue, an attention mechanism is used in the encoder-decoder model, which allows the model to establish a direct relationship between the input and output sequences. This relationship is captured through the use of attention weights, which assign higher weights to the relevant inputs and lower weights to the non-relevant ones, thereby enabling each output to focus on the appropriate input. By using attention, the decoder can access a weighted combination of all the encoder's hidden states, rather than relying solely on the last hidden state of the encoder.

In the attention-based encoder-decoder model, at each time step, the output of the decoder is influenced by the previous outputs, $y_{<t} = \{y_1, y_2, \dots, y_{t-1}\}$, the current decoder hidden state, s_t , and an attention ‘‘context’’ vector, c_t .

$$\begin{aligned} p(y_t | y_1, y_2, \dots, y_{t-1}, x) &= f(s_t, c_t), \\ f(s_t, c_t) &= \text{softmax}(W_s \tilde{s}_t), \\ \tilde{s}_t &= \tanh(W_c [c_t, s_t]). \end{aligned}$$

where the W_c is a learnable weight matrix. The current hidden state, s_t , is determined by the decoder GRU unit, which takes the previous hidden state s_{t-1} , and the last decoder output value, y_{t-1} as input:

$$s_t = GRU(S_{t-1}, y_{t-1})$$

To calculate the context vector, c_t , the attention model proposed by [1] is used. At time step t , the context vector, c_t , is the weighted average over all the encoder hidden states. The weights, $w_{tt'}$, which are the normalized attention scores, $e_{tt'}$, determine the amount of attention to each encoder output.

$$c_t = \sum_{t'=1}^{N_x} w_{tt'} h_{t'},$$

$$\begin{aligned} w_{tt'} &= \frac{\exp(e_{tt'})}{\sum_{k=1}^{N_x} \exp(e_{tk})}, \\ e_{tt'} &= s_t^T W_a h_{t'} \end{aligned}$$

where $e_{tt'}$ is called score function in [1], $h_{t'}$ is the encoder hidden state at time step t' , and W_a is weight matrix. For a more comprehensive understanding of the attention mechanism, see [56].

B. Dataset

To train our neural network model, we employ an 18-month dataset comprising 8,854,325 telematic data points associated with 32,097 trajectories recorded in Manhattan, New York City spanning from January 2015 to June 2016. This dataset is sourced from approximately 4,500 city-owned vehicles, each equipped with telematics devices and managed by the New York City Department of Citywide Administrative Services (NYC DCAS). The telematics devices recorded vehicle positions at roughly 30-second intervals. This data was initially map-matched using an in-house map-matching engine, developed by Alrassy et al. [55]. Trajectories processed through this map-matching engine accounted as the labels for our study. The GPS error statistics including the mean, median and standard deviation of the GPS errors are 15.73m (51.6ft), 6.95m (22.8ft), and 23.13m (75.9ft), respectively. Additionally, the spatial distribution of the average GPS error per road segment is illustrated in Figure 5. As expected, the error has a spatially heterogeneous pattern and the highest error is observed in midtown and downtown of Manhattan due to the existence of tall towers. For the digital map, LION Single Line Street Base map spatial data (version 17D), which is publicly available from the NYC Department of City Planning, is utilized.

C. Pre-processing

To integrate trajectory data into the encoder-decoder model, a series of preprocessing steps are required. The first step is transforming the raw point-based trajectories into a grid-based trajectories. The concept of using a grid representation for maps has its origin in the field of object localization in robotics [57]. It has also found practical applications in space-free vehicle trajectory recovery [49], [50]. Furthermore, it became a valuable strategy in seq2seq map-matching models, facilitating the conversion of the continuous input domain into a discrete domain [45]–[48]. In this procedure, each individual data point was mapped onto non-overlapping square cells, effectively partitioning the entire region into uniform grid cells (Figure 6). During this process, various grid cell sizes were explored. It was observed that employing an excessively small grid size resulted in an extensive number of grid cells, potentially compromising the performance of the seq2seq model. Consequently, a range of grid sizes between 100–200 was tested. The grid size of 150ft was considered the optimal choice, yielding better accuracy. Subsequently, rather than using a sequence of points, each input trajectory is now depicted as a sequence of grid cells, while on the other hand, the output trajectory is a sequence of road segments. Due to the low sampling rate, usually, the length of the input



Fig. 5. Spatial distribution of GPS error aggregated per segment.

trajectory (the count of grid cells) is smaller than the length of the corresponding output trajectory, i.e., the size of the road segment sequence representing the complete route. As a result of the partitioning, the input set yielded a total of 25,146 distinct grids, while the output set comprised 17,965 unique segments.

The second preprocessing step focuses on segmenting lengthy trajectories for training. Encoder-decoder models, constrained by memory limitations, impose a maximum sequence length. When dealing with extensive input sequences, including lengthy trajectories, they often surpass this limit. To resolve this challenge, we split long input trajectories into shorter segments that conform to the model’s constraints. This segmentation addresses the memory issue and also alleviates computational complexity. We have set the maximum trajectory length to 100 and 50 road segments for transformer- and RNN-encoder-decoder model, respectively, and apply a short overlapping between fragments when splitting the trajectories.

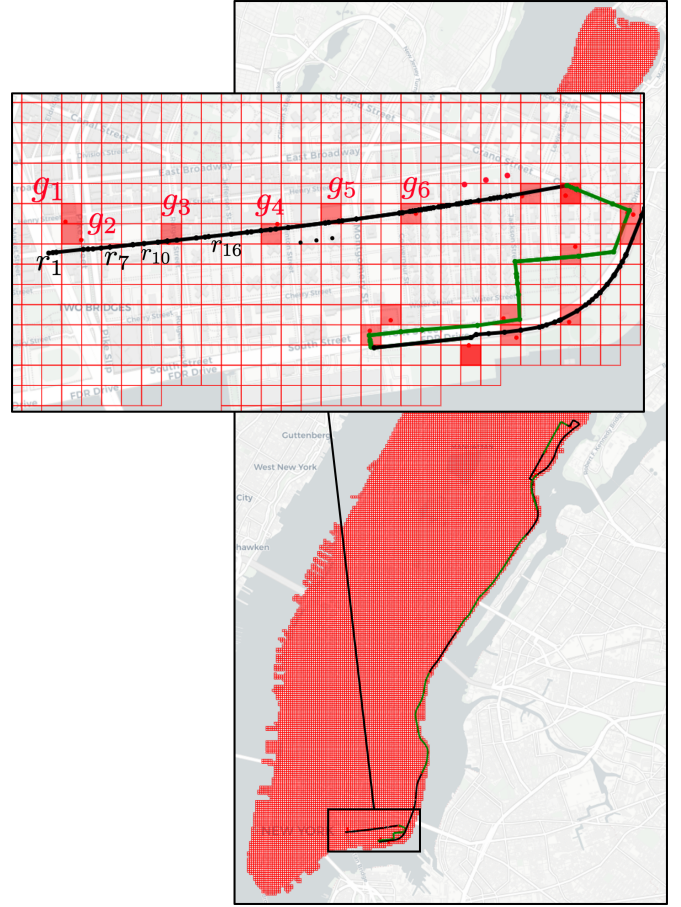


Fig. 6. Trajectory and Grid Representations. For illustration purpose, black and green colors are used to depict the trajectory segments, alternating between the two colors in every other segment.

This strategy helps us comply to the length constraint while with overlapping approach preserves the correlations between the individual trajectory segments. The smaller maximum length is selected for the Bi-GRU encoder-decoder since training the RNN models for long sequences is challenging. Based on the trajectory data and the statistics, it’s observed that, on average, there are approximately 4 road segments between every two consecutive GPS points. To ensure that the maximum length of the road segment sequence does not exceed the limit, we have chosen to set the maximum length of the GPS sequence to 20 GPS points for training the transformer and 8 GPS points for training the RNN model. Example of trajectory segmentation is shown in Figure 6. For illustration purpose, we use black and green colors to depict the trajectory sections, alternating between the two colors in every other section.

D. Implementation Detail

After evaluating different sets, model hyperparameters are configured as follows. The embedding dimension (d_{emb}) is set to 512, while the MLP intermediate dimension (d_{ff}) is set to 2048. We use 8 transformer blocks for both the encoder and decoder, and each multi-head attention block employs 16 linear transformations, resulting in $d_k = 32$. During training,

we utilize the Adam optimizer with a learning rate of 0.0001 and the cross-entropy loss function. The batch size is fixed at 200, and the model undergoes training for a total of 32 epochs. For the RNN model, the embedding dimension is set to 1024. We employ the Adam optimizer with a learning rate of 0.0005 for both the encoder and decoder. Similarly, the batch size is fixed at 200, and the model undergoes training for a total of x epochs reaching to the point that the loss function converges. We implemented the model in Python using the PyTorch library. We trained our models on one machine with NVIDIA RTX 6000 GPUs.

E. Evaluation Metrics

The performance of the model is evaluated using four different metrics, accuracy, length-based accuracy, Jackkard similarity, and Bilingual Evaluation Understudy (BLEU) [58], mathematically described below:

$$\text{Accuracy} = Acc_1 = \frac{1}{N} \sum_{i=1}^N \frac{|\hat{T}_i \cap T_i|}{|T_i|}$$

$$\text{Length-based Accuracy} = Acc_2 = \frac{1}{N} \sum_{i=1}^N \frac{\text{length}(\hat{T}_i \cap T_i)}{\text{length}(T_i)}$$

where T_i and \hat{T}_i are the i th ground truth path and the estimated path in the whole trajectory set T . $|\cdot|$ represents the segment count of the trajectory while $\text{length}(\cdot)$ represents the length of the trajectory in meters.

The Jaccard similarity is a measure of similarity between two sets. Here, we use this metric to compare each trajectory with model estimation. It is defined as the size of the intersection of the two routes composed of road segments divided by the size of their union and yields a value between 0 and 1, where 0 indicates no similarity (no common elements) and 1 indicates complete similarity (identical sets).

$$\text{Jackkard} = J(T_i, \hat{T}_i) = \frac{1}{N} \sum_{i=1}^N \frac{|\hat{T}_i \cap T_i|}{|\hat{T}_i \cup T_i|}$$

BLEU is a metric commonly used to evaluate the quality of machine-generated text, particularly in the context of machine translation. However, in the context of this paper, BLEU is utilized to evaluate the similarity of the predicted segment-based trajectory with the ground truth trajectory. Similar to the text evaluation, here it is assumed to operate by comparing n -grams (contiguous sequences of n road segments) in the candidate and reference trajectories. The intuition behind BLEU is that a good mapping should have similar n -gram statistics to those of the ground truth trajectories. It has two parts, *precision*, and *brevity penalty*. Precision which counts how many contiguous sequences of “ n ” items (n -grams) in the candidate route match those in the reference route and divides this count by the total number of n -grams in the candidate routes and *brevity penalty* that penalizes the short mappings [58].

$$\text{Precision}(\hat{T}_i, T_i) = \frac{\text{count of } n\text{-gram matches between } \hat{T}_i, T_i}{\text{Count of } n\text{-grams in } \hat{T}_i},$$

$$BP = \begin{cases} 1 & |\hat{T}_i| > |T_i| \\ \exp\left(1 - \frac{|\hat{T}_i|}{|T_i|}\right) & |\hat{T}_i| \leq |T_i|, \end{cases}$$

$$\text{BLEU} = BP \exp\left(\frac{1}{n} \sum_{i=1}^n \log(\text{Precision}_i)\right)$$

where n is the maximum n -gram length considered. In this paper, we report the equally weighted average of n -grams for n -values ranging from 1 to 4.

VI. RESULTS

The trajectory data is randomly split into 98% (31,455 trajectories) for training and 2% (642 trajectories) for testing. The average length of trajectories used for testing the model’s performance is 16 kilometers (10 miles). After trajectory segmentation to adhere to the constraint of the maximum length, the data size expands to 272,722 to train the transformer model and 402,361 to train the Bi-GRU encoder-decoder model. The models are trained using the train data set and then evaluated with the test data set. The transformer encoder-decoder model outperformed the Bi-GRU encoder-decoder and resulted in an accuracy (Acc_1) of 75.2%, length-based accuracy (Acc_2) of 76.1%, Jackkard similarity (J) of 78.1%, and BLEU of 75.6%. While, the Bi-GRU encoder-decoder model resulted in the accuracy (Acc_1) of 58.3%, length-based accuracy (Acc_2) of 58.5%, Jackkard similarity (J) of 53.7% and BLEU of 53.9%. Results are summarized in table I. The transformer model reached convergence after 30 epochs, with each epoch completing in 33 minutes. On the other hand, the RNN-based model achieved convergence in 10 epochs, although each epoch took a longer 1632 minutes. However, a closer examination of the inference times for various trajectory lengths, as depicted in Figure 7, reveals that the RNN-based encoder-decoder model exhibits faster inference times than the transformer model. This variance can be attributed to the distinctive architectural characteristics of the models. Generally, the transformers-based encoder-decoder model exhibits more effective and faster convergence compared to the RNN-based counterpart. Several factors contribute to this phenomenon. First, the self-attention layer’s sequential operation complexity is $O(1)$ while the recurrent layers’ sequential operation is $O(n)$. The self-attention layer captures relationships and dependencies between different parts of the input sequence. Then, the number of operations required to connect all positions (or elements) within the sequence remains constant, regardless of the sequence length. This is typically achieved by using matrix operations that can be efficiently paralleled, making self-attention well-suited for capturing long-range dependencies in sequences. A recurrent layer, on the other hand, involves operations that depend on the previous states of the layer. Thus, the computation at each step is dependent on the computation of the previous step. As a result, the number of sequential operations required by a recurrent layer scales linearly with the length of the sequence. This is represented by $O(n)$, where n is the length of the sequence. Second, the complexity per layer of the self-attention layer used in the transformer is $O(n^2d)$ where d is the model dimension (in our case the model embedding dimension). In a self-attention

layer, attention scores are computed between all pairs of positions in the input sequence, resulting in a quadratic complexity with respect to the sequence length n . Additionally, each attention score involves a dot-product computation between two d -dimensional vectors, which contributes to the d factor in the complexity. While the recurrent layer’s complexity is $O(nd^2)$. At each position, there’s a multiplication of a d dimensional vector (the input) with a d dimensional matrix (the recurrent weight matrix), leading to the d^2 factor in the complexity expression and the overall complexity of $O(nd^2)$. Since in our study, the model dimension is larger than the input sequence, thus, the recurrent layer is more complex than the self-attention layer.

Overall, the transformer model has demonstrated promising performance in the map-matching task. However, it should be noted that the deep transformer model benefits significantly from leveraging large trajectory data during training. This enables it to capture the mobility patterns from processing a wealth of trajectories, ultimately leading to its superior performance. Figure 8 presents an example of map-matched results using a transformer-based model (in blue) compared to a cost-based Hidden Markov Model (HMM) map-matching algorithm (in black) for a trajectory from Pearl Street to Battery Park. The Transformer-based model, represented by the blue line, exhibits a more direct and streamlined path, capturing the mobility pattern based on extensive historical data. In contrast, the Cost-based HMM map-matching algorithm, depicted by the black line, suggests a peculiar detour along Beaver Street in the mid-way of the journey. This deviation from the straight path is a characteristic of the HMM’s probabilistic nature, where it may make decisions based on local observations without global context. Figure 9 illustrates another example of a lengthy trajectory that originated at the intersection of Henry Street and Pike Street and concluded at the intersection of East End Ave and FDR Dr. The outcome reveals a substantial alignment between the route matched with the map utilizing a cost-based HMM and the route matched with a transformer-based approach. However, there are a few noticeable discrepancies between the two methods. For instance, in Allen Street, the transformer recommends continuing on a straight path, while the HMM algorithm suggests making a turn onto Hester Street. The former alignment corresponds more closely to the collected GPS points and aligns better with the intuition.

In the map-matching results, additional discrepancies are present, which degrades the quality of the matching process. These discrepancies stem from the manner in which inferences associated with segmented routes are combined. In this study, we employed a brute-force approach for merging the inferences of two adjacent segments with partial overlap; the model retains the first segment and combines the remaining portion of the second segment. This approach represents one of the limitations of our work, and addressing this issue calls for a more rigorous solution.

VII. CONCLUSION

In conclusion, this paper has introduced and demonstrated the effectiveness of a deep-learning model, specifically the

Model	Acc_1	Acc_2	J	BLEU
Transformer	0.752	0.761	0.781	0.756
RNN(BiGRU)	0.583	0.585	0.537	0.539

TABLE I
MODELS’ PERFORMANCE METRICS

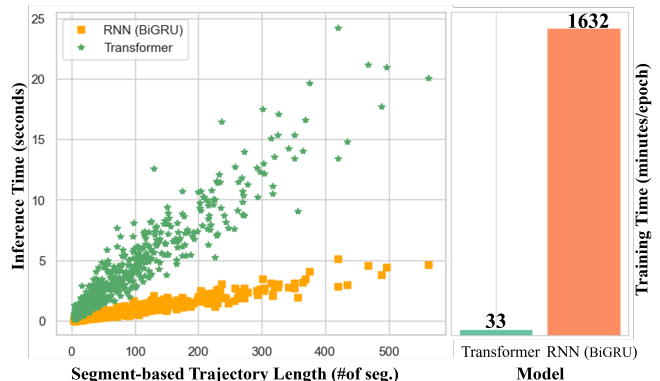


Fig. 7. Training and Inference Time.

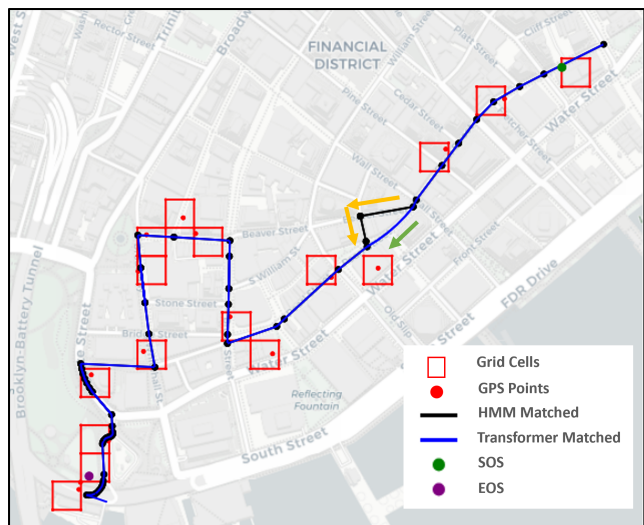


Fig. 8. An example of map-matched results using a Transformer-based model (in blue) compared to a cost-based Hidden Markov Model (HMM) map-matching algorithm (in black) for a trajectory from Pearl Street to Battery Park. The Transformer-based model, represented by the blue line, exhibits a more direct and streamlined path, capturing the mobility pattern based on extensive historical data. In contrast, the Cost-based HMM map-matching algorithm, depicted by the black line, suggests a peculiar detour along Beaver Street in the mid-way of the journey. This deviation from the straight path is a characteristic of the HMM’s probabilistic nature, where it may make decisions based on local observations without global context.

transformer-based encoder-decoder architecture, as a surrogate for advanced map-matching algorithms. This model has shown remarkable capabilities in addressing the challenges posed by noisy GPS data in urban road networks. The encoder in the encoder-decoder framework, is capable in encoding the sequence of noisy GPS points and capturing their autoregressive behavior and spatial correlations. By associating these representations with road network features, the decoder efficiently transforms them into a sequence of road segments, effectively mapping noisy GPS data to navigated routes. Through rigorous training and evaluation on GPS traces collected in Manhattan,

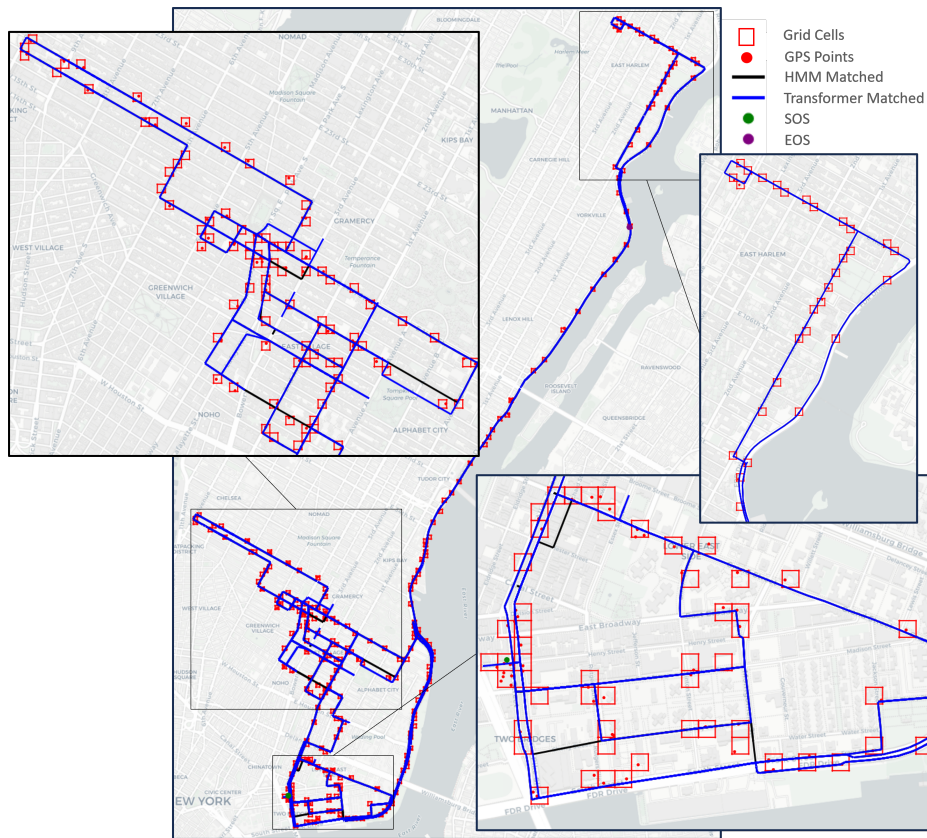


Fig. 9. Example of a lengthy trajectory that originated at the intersection of Henry Street and Pike Street and concluded at the intersection of East End Ave and FDR Dr. The outcome reveals a substantial alignment between the route matched with the map utilizing a cost-based HMM and the route matched with a transformer-based approach.

New York, the model has achieved the highest accuracy rate of 80% compared to the accuracy of the RNN-based encoder-decoder models trained in the urban networks of China reported in the literature. This level of performance aligns with the success of transformer-based encoder-decoder models widely used in natural language processing, further underscoring the model’s promise in translating complex and noisy GPS data into accurate navigational routes within urban road networks. In conclusion, this study has fulfilled its primary objective by developing a deep learning surrogate model that can replicate the complex and computationally intensive processes of advanced map-matching algorithms. This surrogate model offers an efficient alternative to traditional matching methods, significantly enhancing both the speed and accuracy of map-matching tasks. Moreover, its ability to autonomously capture underlying mobility patterns and noise structures within trajectory data contributes to more precise and robust matching results. Ultimately, this research marks a substantial advancement in map-matching techniques, providing a powerful and efficient solution for the identification and tracking of trajectories within intricate and densely populated road networks. The transformer-based encoder-decoder model’s success in this context has promising implications for various applications involving location-based services and urban mobility analysis.

VIII. ACKNOWLEDGMENTS

The authors acknowledge the support from Google and the Tides Foundation under the grant “EMS Resource Deployment Modeling” and the Columbia University Urban Technology Pilot Award. This work was also partially supported by the Center for Smart Streetscapes, an NSF Engineering Research Center, under grant agreement EEC-2133516. Authors also acknowledge Dr. Patrick AIRassy for his help with the original HMM algorithm data processing.

REFERENCES

- [1] M. Batty, K. W. Axhausen, F. Giannotti, A. Pozdnoukhov, A. Bazzani, M. Wachowicz, G. Ouzounis, and Y. Portugali, “Smart cities of the future,” *The European Physical Journal Special Topics*, vol. 214, pp. 481–518, 2012.
- [2] Y. Gao, S. Qian, Z. Li, P. Wang, F. Wang, and Q. He, “Digital twin and its application in transportation infrastructure,” in *2021 IEEE 1st International Conference on Digital Twins and Parallel Intelligence (DTPI)*. IEEE, 2021, pp. 298–301.
- [3] M. Abdel-Aty, O. Zheng, Y. Wu, A. Abdelraouf, H. Rim, and P. Li, “Real-time big data analytics and proactive traffic safety management visualization system,” *Journal of Transportation Engineering, Part A: Systems*, vol. 149, no. 8, p. 04023064, 2023.
- [4] A. J. Khattak, I. Mahdinia, S. Mohammadi, A. Mohammadnazar, and B. Wali, “Big data generated by connected and automated vehicles for safety monitoring, assessment and improvement, final report (year 3),” *arXiv preprint arXiv:2101.06106*, 2021.
- [5] P. Alrassy, A. W. Smyth, and J. Jang, “Driver behavior indices from large-scale fleet telematics data as surrogate safety measures,” *Accident Analysis & Prevention*, vol. 179, p. 106879, 2023.

- [6] S. E. Bibri and J. Krogstie, "Smart sustainable cities of the future: An extensive interdisciplinary literature review," *Sustainable cities and society*, vol. 31, pp. 183–212, 2017.
- [7] N. Lu, N. Cheng, N. Zhang, X. Shen, and J. W. Mark, "Connected vehicles: Solutions and challenges," *IEEE internet of things journal*, vol. 1, no. 4, pp. 289–299, 2014.
- [8] S. Mohammadi, R. Arvin, A. J. Khattak, and S. Chakraborty, "The role of drivers' social interactions in their driving behavior: Empirical evidence and implications for car-following and traffic flow," *Transportation research part F: traffic psychology and behaviour*, vol. 80, pp. 203–217, 2021.
- [9] J. Liu, A. Khattak, and X. Wang, "A comparative study of driving performance in metropolitan regions using large-scale vehicle trajectory data: Implications for sustainable cities," *International Journal of Sustainable Transportation*, vol. 11, no. 3, pp. 170–185, 2017.
- [10] P. Li, M. Abdel-Aty, and J. Yuan, "Using bus critical driving events as surrogate safety measures for pedestrian and bicycle crashes based on gps trajectory data," *Accident Analysis & Prevention*, vol. 150, p. 105924, 2021.
- [11] F. Pinelli, R. Nair, F. Calabrese, M. Berlingerio, G. Di Lorenzo, and M. L. Sbodio, "Data-driven transit network design from mobile phone trajectories," *IEEE Transactions on Intelligent Transportation Systems*, vol. 17, no. 6, pp. 1724–1733, 2016.
- [12] K. Nguyen, J. Yang, Y. Lin, J. Lin, Y.-Y. Chiang, and C. Shahabi, "Los angeles metro bus data analysis using gps trajectory and schedule data (demo paper)," in *Proceedings of the 26th ACM SIGSPATIAL International Conference on Advances in Geographic Information Systems*, 2018, pp. 560–563.
- [13] B. Hui, D. Yan, H. Chen, and W.-S. Ku, "Trajnet: A trajectory-based deep learning model for traffic prediction," in *Proceedings of the 27th ACM SIGKDD Conference on Knowledge Discovery & Data Mining*, 2021, pp. 716–724.
- [14] S. Mohammadi, A. Olivier, and A. Smyth, "Probabilistic prediction of trip travel time and its variability using hierarchical bayesian learning," *ASCE-ASME Journal of Risk and Uncertainty in Engineering Systems, Part A: Civil Engineering*, vol. 9, no. 2, p. 04023011, 2023.
- [15] A. Olivier, S. Mohammadi, A. W. Smyth, and M. Adams, "Bayesian neural networks with physics-aware regularization for probabilistic travel time modeling," *Computer-Aided Civil and Infrastructure Engineering*, 2023.
- [16] A. Olivier, M. Adams, S. Mohammadi, A. Smyth, K. Thomson, T. Kepler, and M. Dadlani, "Data analytics for improved closest hospital suggestion for ems operations in new york city," *Sustainable Cities and Society*, vol. 86, p. 104104, 2022.
- [17] E. L. de Larrea, H. Lam, E. Sanabria, J. Sethuraman, S. Mohammadi, A. Olivier, A. W. Smyth, E. M. Dolan, N. E. Johnson, T. R. Kepler, et al., "Simulating new york city hospital load balancing during covid-19," in *2021 Winter Simulation Conference (WSC)*. IEEE, 2021, pp. 1–12.
- [18] N. Marković, P. Sekuła, Z. Vander Laan, G. Andrienko, and N. Andrienko, "Applications of trajectory data from the perspective of a road transportation agency: Literature review and maryland case study," *IEEE Transactions on Intelligent Transportation Systems*, vol. 20, no. 5, pp. 1858–1869, 2018.
- [19] M. Karaim, M. Elsheikh, A. Noureldin, and R. Rustamov, "Gnss error sources," *Multifunctional Operation and Application of GPS*, pp. 69–85, 2018.
- [20] M. A. Quddus, W. Y. Ochieng, and R. B. Noland, "Current map-matching algorithms for transport applications: State-of-the art and future research directions," *Transportation research part c: Emerging technologies*, vol. 15, no. 5, pp. 312–328, 2007.
- [21] M. Hashemi and H. A. Karimi, "A critical review of real-time map-matching algorithms: Current issues and future directions," *Computers, Environment and Urban Systems*, vol. 48, pp. 153–165, 2014.
- [22] P. Alrassy, *Map Data Integration Technique with Large-Scale Fleet Telematics Data as Road Safety Surrogate Measures in the New York Metropolitan Area*. Columbia University, 2020.
- [23] A. Vaswani, N. Shazeer, N. Parmar, J. Uszkoreit, L. Jones, A. N. Gomez, Ł. Kaiser, and I. Polosukhin, "Attention is all you need," *Advances in neural information processing systems*, vol. 30, 2017.
- [24] M. Kubicka, A. Cela, H. Mounier, and S.-I. Niculescu, "Comparative study and application-oriented classification of vehicular map-matching methods," *IEEE Intelligent Transportation Systems Magazine*, vol. 10, no. 2, pp. 150–166, 2018.
- [25] P. Chao, Y. Xu, W. Hua, and X. Zhou, "A survey on map-matching algorithms," in *Databases Theory and Applications: 31st Australasian Database Conference, ADC 2020, Melbourne, VIC, Australia, February 3–7, 2020, Proceedings 31*. Springer, 2020, pp. 121–133.
- [26] C. E. White, D. Bernstein, and A. L. Kornhauser, "Some map matching algorithms for personal navigation assistants," *Transportation research part c: emerging technologies*, vol. 8, no. 1-6, pp. 91–108, 2000.
- [27] D. Bernstein, A. Kornhauser, et al., "An introduction to map matching for personal navigation assistants," 1996.
- [28] M. A. Quddus, W. Y. Ochieng, L. Zhao, and R. B. Noland, "A general map matching algorithm for transport telematics applications," *GPS solutions*, vol. 7, pp. 157–167, 2003.
- [29] J. S. Greenfeld, "Matching gps observations to locations on a digital map," in *Transportation research board 81st annual meeting*, vol. 22, 2002, pp. 576–582.
- [30] R. Zito, G. D'este, and M. Taylor, "Global positioning systems in the time domain: How useful a tool for intelligent vehicle-highway systems?" *Transportation Research Part C: Emerging Technologies*, vol. 3, no. 4, pp. 193–209, 1995.
- [31] W. Y. Ochieng, M. Quddus, and R. B. Noland, "Map-matching in complex urban road networks," 2003.
- [32] B. Hummel, "Map matching for vehicle guidance," in *Dynamic and Mobile GIS*. CRC Press, 2006, pp. 211–222.
- [33] P. Newson and J. Krumm, "Hidden markov map matching through noise and sparseness," in *Proceedings of the 17th ACM SIGSPATIAL international conference on advances in geographic information systems*, 2009, pp. 336–343.
- [34] C. Y. Goh, J. Dauwels, N. Mitrovic, M. T. Asif, A. Oran, and P. Jaillet, "Online map-matching based on hidden markov model for real-time traffic sensing applications," in *2012 15th International IEEE Conference on Intelligent Transportation Systems*. IEEE, 2012, pp. 776–781.
- [35] H. Koller, P. Widhalm, M. Dragaschnig, and A. Graser, "Fast hidden markov model map-matching for sparse and noisy trajectories," in *2015 IEEE 18th International Conference on Intelligent Transportation Systems*. IEEE, 2015, pp. 2557–2561.
- [36] Y. Lou, C. Zhang, Y. Zheng, X. Xie, W. Wang, and Y. Huang, "Map-matching for low-sampling-rate gps trajectories," in *Proceedings of the 17th ACM SIGSPATIAL international conference on advances in geographic information systems*, 2009, pp. 352–361.
- [37] L. Li, M. Quddus, and L. Zhao, "High accuracy tightly-coupled integrity monitoring algorithm for map-matching," *Transportation Research Part C: Emerging Technologies*, vol. 36, pp. 13–26, 2013.
- [38] M. Quddus and S. Washington, "Shortest path and vehicle trajectory aided map-matching for low frequency gps data," *Transportation Research Part C: Emerging Technologies*, vol. 55, pp. 328–339, 2015.
- [39] M. E. El Najjar and P. Bonnifait, "A road-matching method for precise vehicle localization using belief theory and kalman filtering," *Autonomous Robots*, vol. 19, pp. 173–191, 2005.
- [40] L. Zhao, W. Y. Ochieng, M. A. Quddus, and R. B. Noland, "An extended kalman filter algorithm for integrating gps and low cost dead reckoning system data for vehicle performance and emissions monitoring," *The journal of Navigation*, vol. 56, no. 2, pp. 257–275, 2003.
- [41] S. Kim and J.-H. Kim, "Adaptive fuzzy-network-based c-measure map-matching algorithm for car navigation system," *IEEE Transactions on industrial electronics*, vol. 48, no. 2, pp. 432–441, 2001.
- [42] M. A. Quddus, R. B. Noland, and W. Y. Ochieng, "A high accuracy fuzzy logic based map matching algorithm for road transport," *Journal of Intelligent Transportation Systems*, vol. 10, no. 3, pp. 103–115, 2006.
- [43] E. W. Dijkstra, "A note on two problems in connexion with graphs," in *Edsger Wybe Dijkstra: His Life, Work, and Legacy*, 2022, pp. 287–290.
- [44] G. D. Forney, "The viterbi algorithm," *Proceedings of the IEEE*, vol. 61, no. 3, pp. 268–278, 1973.
- [45] J. Feng, Y. Li, K. Zhao, Z. Xu, T. Xia, J. Zhang, and D. Jin, "Deepmm: deep learning based map matching with data augmentation," *IEEE Transactions on Mobile Computing*, vol. 21, no. 7, pp. 2372–2384, 2020.
- [46] H. Ren, S. Ruan, Y. Li, J. Bao, C. Meng, R. Li, and Y. Zheng, "Mtrajrec: Map-constrained trajectory recovery via seq2seq multi-task learning," in *Proceedings of the 27th ACM SIGKDD Conference on Knowledge Discovery & Data Mining*, 2021, pp. 1410–1419.
- [47] L. Jiang, C.-X. Chen, and C. Chen, "L2mm: learning to map matching with deep models for low-quality gps trajectory data," *ACM Transactions on Knowledge Discovery from Data*, vol. 17, no. 3, pp. 1–25, 2023.
- [48] Y. Liu, Q. Ge, W. Luo, Q. Huang, L. Zou, H. Wang, X. Li, and C. Liu, "Graphmm: Graph-based vehicular map matching by leveraging trajectory and road correlations," *IEEE Transactions on Knowledge and Data Engineering*, 2023.
- [49] S. H. Park, B. Kim, C. M. Kang, C. C. Chung, and J. W. Choi, "Sequence-to-sequence prediction of vehicle trajectory via lstm encoder-

- decoder architecture,” in *2018 IEEE intelligent vehicles symposium (IV)*. IEEE, 2018, pp. 1672–1678.
- [50] J. Wang, N. Wu, X. Lu, W. X. Zhao, and K. Feng, “Deep trajectory recovery with fine-grained calibration using kalman filter,” *IEEE Transactions on Knowledge and Data Engineering*, vol. 33, no. 3, pp. 921–934, 2019.
- [51] J. Feng, Y. Li, C. Zhang, F. Sun, F. Meng, A. Guo, and D. Jin, “Deep-move: Predicting human mobility with attentional recurrent networks,” in *Proceedings of the 2018 world wide web conference*, 2018, pp. 1459–1468.
- [52] I. Sutskever, O. Vinyals, and Q. V. Le, “Sequence to sequence learning with neural networks,” *Advances in neural information processing systems*, vol. 27, 2014.
- [53] D. Grechishnikova, “Transformer neural network for protein-specific de novo drug generation as a machine translation problem,” *Scientific reports*, vol. 11, no. 1, p. 321, 2021.
- [54] J. L. Ba, J. R. Kiros, and G. E. Hinton, “Layer normalization,” *arXiv preprint arXiv:1607.06450*, 2016.
- [55] P. Alrassy, J. Jang, and A. W. Smyth, “Obd-data-assisted cost-based map-matching algorithm for low-sampled telematics data in urban environments,” *IEEE Transactions on Intelligent Transportation Systems*, vol. 23, no. 8, pp. 12 094–12 107, 2021.
- [56] M.-T. Luong, H. Pham, and C. D. Manning, “Effective approaches to attention-based neural machine translation,” *arXiv preprint arXiv:1508.04025*, 2015.
- [57] A. Milstein, “Occupancy grid maps for localization and mapping,” *Motion planning*, pp. 381–408, 2008.
- [58] K. Papineni, S. Roukos, T. Ward, and W.-J. Zhu, “Bleu: a method for automatic evaluation of machine translation,” in *Proceedings of the 40th annual meeting of the Association for Computational Linguistics*, 2002, pp. 311–318.